C44

The carotid body-mediated ventilatory response to insulin-induced hypoglycaemia in anaesthetized rats

I. Bin-Jaliah and P. Kumar

Department of Physiology, The Medical School, University of Birmingham, Birmingham B15 2TT, UK

Peripheral chemoreceptors may play an important role in the, neuroendocrine-mediated, control of glucose homeostasis (Koyama *et al*. 2000) through a hypoglycaemia-induced stimulation of carotid body glomus cells (Pardal & Lopez-Barneo, 2002). We postulated that carotid body stimulation by hypoglycaemia should therefore, like hypoxia, also induce hyperventilation.

Adult Wistar rats (300–370 g) were anaesthetised with pentobarbitone sodium (60 mg kg^{-1}, I.P.). Spontaneous ventilation ($\dot{V}_E$) was measured as integrated tracheal airflow and blood pressure monitored from an indwelling arterial catheter. All animals were humanely killed at the end of the experiment. Data are expressed as means ± S.E.M. and significance ($P < 0.05$) tested with regression analysis and ANOVA.

Basal blood glucose was similar in both sham-operated, control (sham; $n = 7$) and carotid sinus nerve sectioned (CSNX; $n = 7$) animals (6.0 ± 0.1 and 6.3 ± 0.1 mmol l^{-1} respectively; $P > 0.05$). Insulin infusion (0.4 U min^{-1} kg^{-1}) lowered blood glucose concentration in both groups ($P < 0.0001$) to 3.3 ± 0.1 mmol l^{-1} in sham and to 3.6 ± 0.1 mmol l^{-1} in CSNX animals, values that were not different from each other ($P > 0.07$). Hypoglycaemia increased $\dot{V}_E$ in sham animals from 512.40 ± 7.58 to 613.33 ± 11.28 ml min^{-1} kg^{-1} ($P < 0.001$) but without any significant change in the arterial partial pressure of CO_2 (P_{a,CO_2}) or pH. In contrast, $\dot{V}_E$ did not increase in CSNX animals during hypoglycaemia and P_{a,CO_2} increased from 44.4 ± 0.7 to 48.7 ± 0.9 mmHg and pH decreased from 7.375 ± 0.007 to 7.348 ± 0.007 ($P < 0.003$ for both). In a separate group of sham and CSNX animals ($n = 4$ in each group), oxygen consumption ($\dot{V}_{O_2}$) was measured using spirometry. Basal levels of $\dot{V}_{O_2}$ (28.22 ± 2.72 and 34.39 ± 3.16 ml min^{-1} kg^{-1} STPD; $P > 0.1$) and $\dot{V}_E/\dot{V}_{O_2}$ ratios (16.69 ± 2.24 and 12.42 ± 1.55; $P > 0.1$) were not significantly different in sham and CSNX animals. During hypoglycaemia, $\dot{V}_{O_2}$ in both groups was significantly and similarly increased from the basal levels by 2.36 ± 0.3-fold in sham and 2.22 ± 0.2-fold in CSNX. The $\dot{V}_E/\dot{V}_{O_2}$ ratio during hypoglycaemia was decreased significantly in CSNX animals to around half its basal value ($P < 0.01$) but remained unchanged in sham animals ($P > 0.05$).

These results demonstrate that hypoglycaemia can induce, as predicted, a carotid body-dependent increase in ventilation and in addition, we show that, *in vivo*, this response is directly proportional to the increased metabolism induced. Whether the stimulus is hypoglycaemia *per se* or some other factors related to the increased metabolism is not known.

Koyama Y *et al.* (2000). *Diabetes* **49**, 1434–1442.

Pardal R & Lopez-Barneo J (2002). *Nat Neurosci* **5**, 197–198.

We acknowledge the financial support of King Khalid University, Saudi Arabia and the British Heart Foundation.

All procedures accord with current UK legislation.

C45

pH regulation in sympathetic neurons of the rat middle cervical stellate ganglion

C. Paul Plested, Nina L. Muirhead and Keith J. Buckler

University Laboratory of Physiology, University of Oxford, Oxford OX1 3PT, UK

Both myocardial ischaemia and anoxia cause massive noradrenaline release from cardiac sympathetic nerves. It has been hypothesised that this is mediated by leakage of noradrenaline from secretory vesicles and the activation of Na^+–H^+ exchange (NHE) leading to a rise in cytosolic Na^+ and noradrenaline causing a reversal of Na^+–noradrenaline co-transport (efflux) by uptake 1. The proposed role of NHE in this scheme is based upon the observation that amiloride analogues inhibit ischaemia- or anoxia-induced noradrenaline release (Kurz *et al.* 1996; Levi & Smith 2000). Surprisingly, there have been no direct studies of the effects of anoxia or ischaemia on NHE activity in sympathetic neurons; indeed there is little data on the role or function of NHEs in sympathetic neurons. Therefore, we have investigated the effect of anoxia on the regulation of intracellular pH (pH_i) in sympathetic neurons isolated from the middle cervical stellate ganglia (MCSG) of the rat. This ganglion complex represents the major source of postganglionic sympathetic nerves that supply the heart.

MCSG were excised from humanely killed 11- to 13-day-old Sprague-Dawley rat pups. Sympathetic neurons were disassociated from the ganglia by collagenase–trypsin digestion and were cultured under 5 % CO_2–air at 37 °C on glass coverslips coated with poly-L-lysine. Cells were used within 4 days and pH_i was determined using the pH indicators BCECF or SNARF-1.

The mean pH_i of single neurons was 7.07 ± 0.07 (± S.E.M., $n = 76$) when perfused with a Hepes buffered Tyrode solution (HBTS pH 7.4 at 37 °C). Under these conditions there was a rapid recovery of pH_i from an imposed acid load (NH_3/NH_4^+ prepulse). Recovery from an acid load was prevented by the NHE inhibitor amiloride (1.5 mM) and under Na^+-free conditions (NMDG substituted). Exposure to anoxic conditions (HBTS bubbled for >1 h with N_2 gas + 1 mM $Na_2S_2O_4$) caused a sustained decrease in pH_i within 10 min (ΔpH_i −0.23 ± 0.02 pH units, Student's paired *t* test $P < 0.001$, $n = 19$). Under anoxic conditions there was substantially reduced pH_i recovery from an imposed acid load.

These data confirm the presence of NHE in sympathetic neurons and demonstrate that NHEs play a key role in pH_i regulation under normoxic conditions. However, during anoxia NHE activity appears to be markedly suppressed not activated. This observation is contrary to the hypothesis that neuronal NHE activity is increased during anoxia/ischaemia. The effects of other aspects of ischaemia upon neuronal NHE activity and the mechanisms of pH_i regulation in sympathetic neurons are currently under further investigation.

Kurz T *et al.* (1996). *Naunyn-Schmiedeburgs Arch Pharmacol* **354**, 7–16.

Levi R & Smith NCE (2000). *J Pharmacol Exp Ther* **292**, 7–16.

This work was funded by the Wellcome Trust.

All procedures accord with current UK legislation.

C46

Spatial aspects of aortic pulse wave transmission in the anaesthetised rabbit

T.A. Sears and D. Banks*

*School of Biomedical Sciences, King's College London and *Department of Biomedical Sciences, Open University, Milton Keynes, UK*

The temporal profile of the aortic pulse wave has been given much attention, for the information it contains about either local blood flow, or the presence of wave reflections indicating the functional status of peripheral vascular beds. However, the changing spatial distribution of the wave as it propagates appears to be ignored, yet this could reveal discontinuities in transmission due to branching and sites of reflection.

In eight male(2.5–3.5 kg) anaesthetized, spontaneously breathing rabbits (sodium pentobarbitone, 50.0 mg kg^{-1} I.P. followed by infusion at 15–25 mg kg^{-1} h^{-1}, I.V.), we recorded aortic blood pressure sequentially at multiple sites with a high fidelity, transducer-tipped catheter (Gaeltec 4F, diam. 1.2 mm) bearing 5.0 mm markings. This was advanced in 5.0 or 10.0 mm steps, through the left femoral artery as far as the aortic arch (240–260 mm), with recording for 10–20 s at each site, sampling at 1024 Hz. Also recorded were the diaphragm EMG, airflow, alveolar CO_2 and the ECG (chest lead) together with a QRS-event pulse. All data were continuously acquired to hard disk using a CED 1401-*plus* interface and Spike2 v4 software. The rabbit was killed by an overdose of anaesthetic and the final position of the transducer defined in relation to the crest of the aortic arch. Off line, the event pulse was used to derive 250 ms duration, post-QRS-event averages encompassing one complete pulse wave at each recording site. The data were exported to a spreadsheet and transposed, and with Origin software, plots were made of the spatial distribution of pressure along the aorta at 1.0 ms intervals. The combined colour and symbol coding allowed superimposition of up to 40 plots at selected times to reveal transmission of a complete pulse wave comprising a total of 250 plots. Below, a selection of 5 plots illustrate certain principal features of aortic pulse wave transmission revealed by this approach; for simplicity only those occurring during systole are shown.

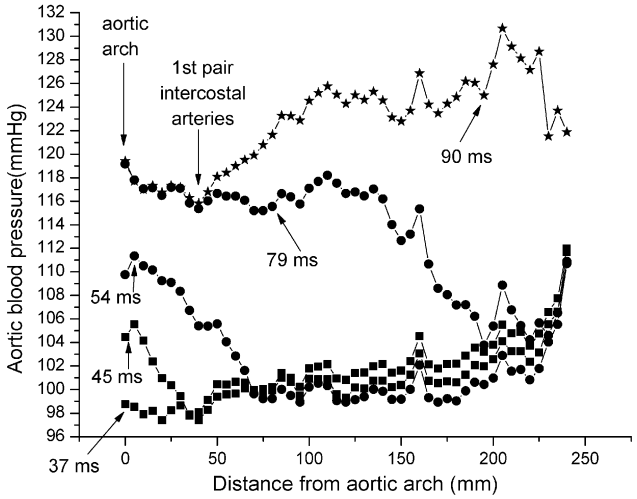

Figure 1. Spatial distribution of the pulse wave following the QRS-event pulse

Figure 1 shows the spatial distribution of the pulse wave at the times indicated following the QRS-event pulse. Note (a) in the 45 ms plot, the rapid decrement of the pulse wave over the initial 25–30 mm of descending aorta which is branch-free; (b) in the 79 ms plot the plateau of pressure extending by then 140 mm along the aorta; and (c) at 90 ms, a major secondary rise in pressure, a reflection which earlier (not shown) had arisen near the thoracico–abdominal boundary (120 mm) and by back transmission had reached the first pair of intercostal arteries.

Thus, by the use of adequate frequency and spatial sampling, new aspects of pulse wave transmission can be revealed.

All procedures accord with current UK legislation.